Inorganic Chemistry
Article
Cite This: Inorg. Chem. 2019, 58, 9773−9784
pubs.acs.org/IC

Metal−Organocatalyst for Detoxification of Phosphorothioate Pesticides: Demonstration of Acetylcholine Esterase Activity

Amanpreet Singh,[†] Pushap Raj,[†] Ajnesh Singh,[‡] Jan J. Dubowski,[§] Navneet Kaur,*[,∥] and Narinder Singh*[,†]

[†]Department of Chemistry, Indian Institute of Technology Ropar, Punjab 140001, India

[‡]Department of Applied Sciences and Humanities, Jawaharlal Nehru Govt. Engineering College, Sundernagar, Mandi (H.P.), 175018, India

[§]Laboratory for Quantum Semiconductors and Photo-based Biotechnology, Interdisciplinary Institute for Technological Innovation (3IT), CNRS UMI-3463, Department of Electrical and Computer Engineering, Universite de Sherbrooke, 3000 Boulevard de l'Université, Sherbrooke, QC J1K 0A5, Canada

[∥]Department of Chemistry, Panjab University, Chandigarh, 160014, India

Supporting Information

ABSTRACT: In recent years, transition metal complexes have been developed for catalytical degradation of a phosphate ester bond, particularly in RNA and DNA; however, less consideration has been given for development of complexes for the degradation of a phosphorothioate bond, as they are the foremost used pesticides in the environment and are toxic to human beings. In this context, we have developed copper complexes of benzimidazolium based ligands for catalytical degradation of a series of organophosphates (parathion, paraoxon, methyl-parathion) at ambient conditions. The copper complexes (assigned as **N1**−**N3**) were characterized using single X-ray crystallography which revealed that all three complexes are mononuclear and distorted square planner in geometry. Further, the solution state studies of the prepared complexes were carried out using UV−visible absorption, fluorescence spectroscopy, and cyclic voltametry. The complexes **N1** and **N2** have benzimidazolium ionic liquid as base attached with two 2-mercapto-benzimidazole pods, whereas complex **N3** contains a nonionic ligand. The synthesized copper complexes were evaluated for their catalytic activity for degradation of organophosphates. It is interesting that the complex containing the ionic ligand efficiently degrades phosphorothioate pesticides, whereas complex **N3** was not found to be appropriate for degradation due to a weaker conversion rate. The organophosphate degradation studies were monitored by recording absorbance spectra of parathion in the presence of catalyst, i.e., copper complexes with respect to time. The parathion was hydrolyzed into *para*-nitrophenol and diethyl thiophosphate. Moreover, to analyze the inhibition activity of the pesticides toward acetylcholine esterase enzyme in the presence of prepared metal complexes, Ellman's assay was performed and revealed that, within 20 min, the inhibition of acetylcholine esterase enzyme decreases by up to 13%.

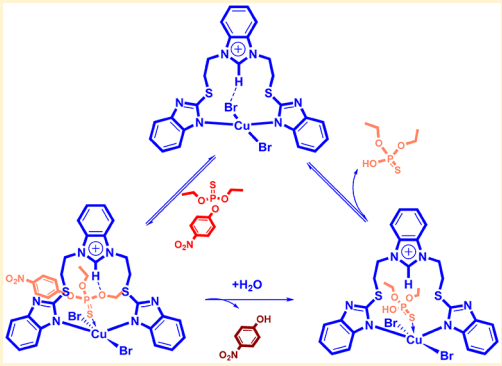

INTRODUCTION

Phosphorothioates are used as pesticides to increase the cultivation in the agriculture sector; their major disrepute is found as chemical warfare agents.[1−8] The recent use of organophosphate (OP) compounds as chemical warfare agents in the Syria war makes constraint to the world. Therefore, the catalyst for degradation of these super toxic chemicals at environment conditions is gaining remarkable interest.[9−18] Phosphorothioates are neurotoxins that bind irreversibly with acetylcholinesterase enzyme and inhibit an important enzymetic conversion from acetylcholine to choline which is a necessary neurotransmitter.[19−23] It is well documented that phosphorothioates bind with acetylcholinesterase enzyme through the hydroxyl group of serine amino acid present in the enzyme.[22−29] It is interesting that serine in free state does not react, whereas the serine residue of acetylcholinesterase protein efficiently binds with phosphorothioate. It means that supramolecular interaction[30−32] of organophosphates with acetylcholinesterase also plays an important role in the hydrolysis process. Such kind of interaction increases the electrophilicity of the phosphate center which results in the increased rate of reaction between the serine residue and OPs. Various enzymes such as organophosphorus hydrolase (OPH), organophosphate-degrading enzyme from agrobacterium radiobacter (OpdA), methyl parathion hydrolase (MPH), and glycerophosphodiesterase (GpdQ) are known for phosphate ester hydrolysis that are having high catalytic efficacy due to

Received: March 18, 2019
Published: July 18, 2019

   DOI: 10.1021/acs.inorgchem.9b00770

their tendency to interact with a substrate through supramolecular interactions.[33−38] Therefore, to achieve a high rate of hydrolysis using an artificial or synthetic catalyst, the strong interaction between substrate and catalyst is required.[39,40] For this purpose, ionic liquids are promising candidates, as these compounds are well-known for catalysis through activating the carbonyl carbon.[41−46] To develop the catalyst for degradation of pesticides, ionic and other noncovalent interactions should be strong enough to increase the electrophilicity of the phosphorus center of OPs.[47] This enhancement of electrophilic character will favor the addition of water and removal of the withdrawing group. Moreover, the interaction of organophosphates with metal ions favors the hydrolysis process. For this purpose, various metal oxides were developed with their own limitations such as a process being stoichiometric, not catalytic. Also, the metal oxides have less possibility of tunability to increase the reaction rate. Recently, Farha et al. have developed a porous zirconium organic framework for encapsulation and degradation of organophosphates.[10,48−51] These porous materials efficiently degrade the phosphorothionate into less toxic byproducts. Our group has also developed some metal complexes and metal organic polymers for sensing and degradation of pesticides.[52−55] These metal complexes were capable of detecting pesticides by fluorescence spectroscopy; however, they could not proceed for a degradation process. Previously, we developed a copper-organic two-dimensional polymer of benzimidazolium zwitterion that catalyzes the degradation process of OPs. The self-degradation of such a framework by reacting with free phosphate ion was its major disadvantage. Dissociation of the complex causes removal of the zwitterion ligand by the cation displacement assay which results in heightening of the fluorescence intensity. The process of degradation was stoichiometric, not catalytic. From this work, we have taken a lead that the combination of benzimidazolium zwitterion and the copper ion is proficient to detoxify OPs. In another work, ionic conjugates of benzimidazolium dipodal and ionic surfactants were developed for the same purpose.[2] All of these work only to decontaminate the OPs in an aqueous medium. However, an antidote for its detoxification by reactivation of acetylcholine esterase is still our goal. As acetylcholine esterase binds strongly with OPs; it is not easy to extract OPs from the active site of the enzyme. This could be achieved with some organocatalysts, as well as metal complexes. Here, we took both catalytic centers into consideration by making a complex of benzimidazolium with metal. By putting one step forward toward this direction, we have developed a copper(II) ion complex of benzimidazolium based on a dipodal receptor that was further explored for catalytic degradation reactions. The advantage of this nitrogen donor ligand involved stronger binding affinity toward copper(II) ion which restricts extraction of copper by phosphate derivatives.[56] Moreover, a benzimidazolium unit attached with a dipodal receptor provides another catalytic site which enhances the hydrolysis process. To confirm the involvement of the benzimidazolium unit, another complex (**N3**) was synthesized, having a similar geometry and the same metal ion, except for the benzimidazolium unit, which was replaced by a nonionic molecule. It is interesting that complex (**N3**) showed a negligible catalytic activity as compared to **N1** and **N2**. The kinetics of the degradation process was analyzed using UV−visible absorption spectroscopy.

■ EXPERIMENTAL SECTION

Material. Copper perchlorate, copper chloride, potassium carbonate, 2,2′-bis(bromomethyl)-1,1′-biphenyl, 2-mercaptobenzimidazole, 2-mercaptobenzothiazole, benzimidazole, and dibromoethane were purchased from Sigma-Aldrich and used without further purification. Due to their explosive nature, the perchlorate salts may be harmful upon ingestion or absorption through the skin. These compounds may cause irritation to the skin, respiratory tract, and eyes. Hence, proper protection and care should be taken while using them. All the organophosphate pesticides were bought from Sigma-Aldrich and used as received. ***Caution!*** *Due to the high toxicity of pesticides, precautions were taken as suggested in the Sigma-Aldrich safety data sheet.* Milli-Q water was used to prepare all the aqueous solutions. Acetonitrile and deuterated solvents were purchased from Merck and Sigma-Aldrich, respectively.

Methods. The ^{1}H NMR, ^{13}C NMR, and ^{31}P NMR spectra of prepared compounds were noted on a Jeol Instrument operating at 400 MHz for ^{1}H NMR, at 100 MHz for ^{13}C NMR, and at 160 MHz for ^{31}P NMR. The chemical shifts were recorded in ppm relative to tetramethylsilane as an internal reference. A PerkinElmer L55 Spectrophotometer was used to conduct the fluorescence measurements at room temperature with a fixed scanning speed and emission slit width (10 nm). UV−visible absorption titrations were performed using a Shimadzu spectrophotometer UV-2600. The concentration of the degraded product was calculated using gas chromatography from Shimadzu (GC-2010). The pH measurement was carried out on the ME/962P instrument. A Fisons CHN analyzer was used for elemental analyses. The cyclic voltammetry studies were carried out on a Metrohm instrument.

Evaluation of Photophysical Properties. All spectroscopic experiments were performed at 25 °C in the pure aqueous medium. The stock solutions of ligand **L1** (10 μM) and copper salts (1 mM) were prepared in distilled water, whereas the solution of the **L2** ligand (10 μM) was prepared in DMSO:water (20:80) which was further diluted as per the need of experiments. The change in absorbance and fluorescence intensity was observed with stepwise addition of the copper salt solution. Binding studies were carried out in an aqueous solution buffered at pH 8.0 using Tris buffer. The sample was prepared in a volumetric flask and sonicated for 5 min to attain an equilibrium before recording the spectra. All the experiments were repeated for three times, and errors in experiments were calculated using a standard deviation method.

Cyclic Voltammetry. The aqueous stock solutions of complexes **N1** and **N2** at a concentration of 10 μM were prepared in Tris buffer at pH 8, which was further diluted as per the requirement of experiments. Due to the insolubility of complex **N3** in water, its solution was prepared in 70:30 water/DMSO. Tetrabutylammonium iodide was used as electrolyte. The current was measured by varying the potential in the range from 0.55 to −1.1 V. The cyclic volumetric graph was recorded by varying the scan rate from 50 to 250 mV s^{-1}.

Method for Calculation of the Rate of Hydrolysis. The solutions of phosphorothioates were prepared in water up to 1 mM concentrations which were further diluted as per the need of the experiment. To the aqueous solution of complex **N1** and **N2** (both are 10 μM) buffered at pH 8.0 using Tris buffer was added parathion (100 μM). The solutions were shaken vigorously before recording the absorbance spectra that was recorded after a short interval of time. The concentration of the degraded product was determined from the absorbance intensity that was further used to analyze the binding constant. The effect of substrate concentration and pH on the rate of hydrolysis was evaluated. Another catalytic parameter such as k_{cat} and catalytic efficiency was determined using a Lineweaver−Burk plot.

Acetylcholine Esterase Activity Analysis. The residual AChE activity was determined on a microplate reader infinite M200PRO (TECAN). AChE activities were monitored to control activity, whereas the data are represented as % of control. We have used diethylchlorophosphate and diethylcyanophosphate as enzyme inhibitor rather than parathion or paraoxon, because of their interference in absorbance intensity at 412 nm in the Ellman assay.

DOI: 10.1021/acs.inorgchem.9b00779

Scheme 1. Synthesis Scheme of Compound 1, Ligands L1 and L2

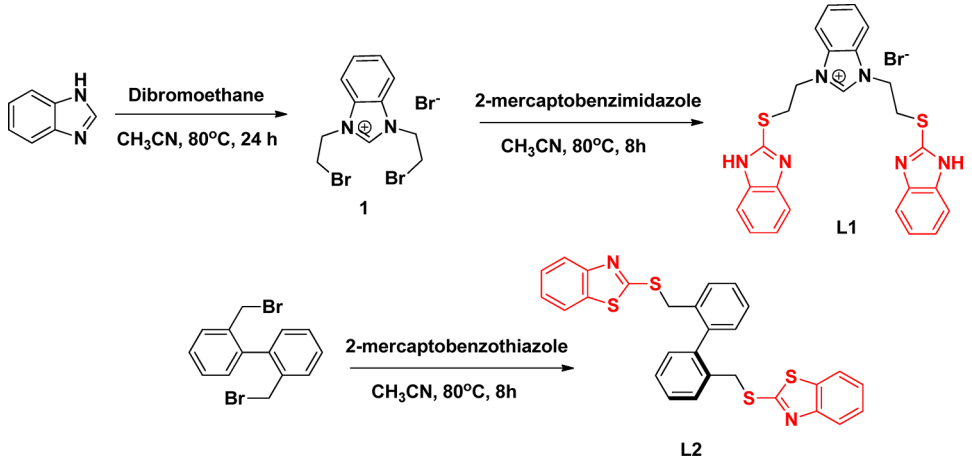

Scheme 2. Chemical Structure of Complexes N1, N2, and N3

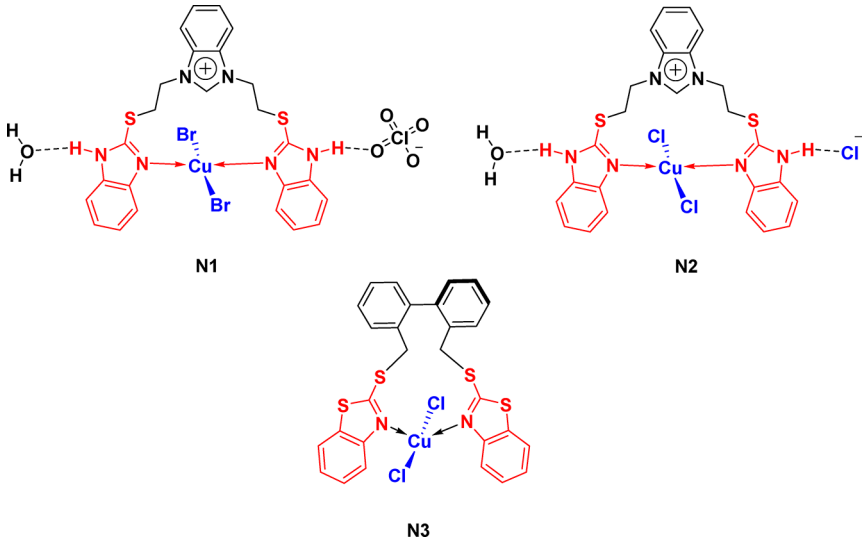

Ellman solution for the detoxification assays of phosphorothioate by metal complexes was prepared by dissolving acetylthiocholine iodide (200 mg, 0.7 mmol), 5,5′-dithiobis(2-nitrobenzoic acid) (100 mg, 0.25 mmol), and sodium bicarbonate (50 mg) in 25 mL of Tris buffer (pH 8). A 10-fold dilution of this solution was then carried out.

X-ray Structure Determination. The diffraction data for all the copper complexes were collected on a Bruker D8 Venture Photon 100 CMOS diffractometer at 293 K using mirror-monochromatized Mo−Kα radiation. The diffraction spots were measured using a counting time of 10 s, and the crystals were positioned at 50 mm from the CCD. The APEX II program was used for data reduction and multiscan absorption. The structures were solved by the direct method with the SIR97 program and refined using SHELXL-97. Anisotropic thermal parameters were used for all non-H atoms. All other calculations were performed using WinGX and PARST. The ORTEP diagrams were drawn using ORTEP3 and OLEX2. The related crystallographic information can be obtained from the Cambridge Crystallographic Data center (CCDC) (CCDC Nos. 1818792−1818794).

Synthesis of Compound 1. Compound **1** was synthesized using our previously developed procedure (Scheme 1).[57] In brief, the benzimidazole (2.36 g, 20 mmol) and dibromoethane (17.12 mL, 200 mmol) were first dissolved in acetonitrile (100 mL), and the resulting solution was refluxed for 24 h. On completion of the reaction, the volatiles were evaporated using a rotary evaporator. The resulting crude mixture was washed with $CHCl_3$ and finally recrystallized in CH_3OH which gave colorless crystals (3.58 g). Yield = 86%. ^{1}H NMR (400 MHz, DMSO-d_6) δ (ppm) = 4.04 (t, J = 8.0 Hz, 4H, CH_2), 5.01 (t, J = 8.0 Hz, 4H, CH_2), 7.69 (d, 2H, ArH), 8.17 (d, 2H, ArH), 10.07 (s, 1H, CH); ^{13}C NMR (100 MHz, DMSO-d_6) δ (ppm) = 31.6, 48.7, 114.4, 127.5, 131.3, 143.9. Anal. Calcd for $C_{11}H_{13}Br_3N_2$: C, 31.99; H, 3.17; N, 6.78. Found: C, 31.95; H, 3.18; N, 6.81.

Synthesis of Ligand L1. Compound **1** (410 mg, 1 mmol) was dissolved in dry CH_3CN and heated at 80 °C for 30 min. 2-Mercaptobenzimidazole (300 mg, 2 mmol) was added to the saturated solution of compound **1**, and the resulting solution was refluxed for 8 h. The reaction was monitored using TLC; after 8 h, the product was separated out as a white powder which was washed with hot chloroform. The resulting white powder constitutes clean ligand **L1**. Yield = 85%. ^{1}H NMR (400 MHz, DMSO-d_6 δ (ppm) = 3.99 (t, J = 8.0 Hz, 4H, CH_2), 4.96 (t, J = 8.0 Hz, 4H, CH_2), 7.03 (dd, J = 8.0 Hz, 2H, ArH), 7.30 (d, J = 8.0 Hz, 4H, ArH), 7.54−7.51 (m, 6H, ArH, NH), 8.04 (d, J = 8.0 Hz, 2H, ArH), 10.09 (s, 1H, CH). ^{13}C NMR (100 MHz, DMSO-d_6) δ (ppm) = 149.1, 143.6, 136.2, 131.3, 127.1, 126.6, 123.9, 122.7, 114.9, 114.1, 113.9, 109.9, 46.9, 31.7. Anal. Calcd for $C_{25}H_{23}BrN_6S_2$: C, 54.44; H, 4.20; N, 15.24, Found: C, 54.48; H, 4.18; N, 15.22.

Synthesis of Ligand L2. Ligand **L2** was synthesized using a similar method as that adopted for ligand **L1**. In a round-bottom flask, 2,2′-bis(bromomethyl)-1,1′-biphenyl (340 mg, 1 mmol) was dissolved in 50 mL of acetonitrile. To the saturated solution was added 300 mg of 2-mercaptobenzothiazole (2 mmol), and resulting mixture

DOI: 10.1021/acs.inorgchem.9b00779

was refluxed for 8 h. The product was separated out as a light-yellow colored compound which filtered out and washed with diethyl ether. The resulting yellow compound constitutes pure ligand **L2**. Yield = 89%. ^{1}H NMR (400 MHz, DMSO-d_6) δ (ppm) = 4.25 (d, J = 12.0 Hz, 2H, CH_2), 4.45 (d, J = 12.0 Hz, 2H, CH_2), 7.21 (t, 2H, ArH), 7.29−7.33 (m, 6H, ArH), 7.38 (t, J = 8.0 Hz, 2H, ArH), 7.59 (t, J = 8.0 Hz, 2H, ArH), 7.75 (d, J = 8.0 Hz, 2H, ArH), 7.89 (d, J = 8.0 Hz, 2H, ArH), ^{13}C NMR (100 MHz, DMSO-d_6) δ (ppm) = 166.2, 152.9, 140.2, 135.1, 134.3, 130.6, 130.5, 128.9, 128.3, 126.9, 125.1, 122.3, 121.7, 35.7. Anal. Calcd for $C_{25}H_{23}BrN_6S_2$: C, 65.59; H, 3.93; N, 5.46. Found: C, 65.61; H, 3.89; N, 5.49.

Synthesis of Copper Complex N1. In a round-bottom flask, copper perchlorate (89 mg, 0.5 mmol) was added to the saturated solution of ligand **L1** (275 mg, 0.5 mmol) in distilled water, and the mixture was heated at 60 °C for 20 min. The blue crystals were obtained after 10 h, which were found to be suitable for single crystal data collection. Yield = 55%. Anal. Calcd for $C_{25}H_{25}Br_2ClCuN_6O_5S_2$: C, 36.96; H, 3.10; N, 10.34 Found: C, 37.04; H, 2.95; N, 10.35.

Synthesis of Copper Complex N2. Complex **N2** was synthesized using a similar method as that for **N1**; copper(II) chloride was used instead of copper perchlorate. Blue colored crystals were grown after 12 h which were found to be suitable for single crystal data collection. Yield = 64%. Anal. Calcd for $C_{25}H_{25}Cl_3CuN_6O_1S_2$: C, 45.53; H, 3.82; N, 12.74 Found: C, 45.45; H 3.50; N, 12.66.

Synthesis of Copper Complex N3. Complex **N3** was synthesized by reacting copper chloride (50 mg, 0.5 mmol) and ligand (100 mg) **L2** in methanol. The resulting mixture was refluxed for 1 h and cooled down to room temperature. Blue crystals grew after 36 h in 60% yield which were suitable for single crystal data collection. Yield = 58%. Anal. Calcd for $C_{28}H_{20}Cl_2CuN_2S_4$: C, 51.97; H, 3.12; N, 4.33. Found: C, 51.56; H, 2.97; N, 4.28.

■ RESULTS AND DISCUSSION

Synthesis and Characterization of Metal Complexes. Ligand **L1** was synthesized using our previously reported method. Earlier, we constructed fluorescence aggregates of **L1** by interacting it with anionic surfactants that were further explored as a fluorescence sensor mimicing chemical warfare agents (diethyl chlorophosphate). It was observed that ligand **L1** interacts with diethyl chlorophosphate (DCP) through hydrogen bonding and efficiently degrades it in 1 h. Here, we have designed complexes **N1** and **N2** in such a way that the benzimidazolium unit is still free to interact with organophosphate derivatives through hydrogen bonding (Scheme 2). Such kinds of pincer ligands based complexes are well-known for catalytic applications.[58−60] Along with the insertion of copper ion in the pocket of the dipodal receptor, this will provide ionic interaction to organophosphate which enhances the electrophilicity of the phosphorus center and increases the rate of the hydrolysis process. Keeping this in mind, complexes **N1** and **N2** were synthesized by reacting ligand **L1** in distilled water with copper perchlorate and copper chloride, respectively. The mixture was heated for 20 min and cool down to room temperature. It was interesting that, in the case of **N1**, the counterion (bromide) present in **L1** coordinated with copper metal ion, whereas perchlorate ion interacted with the benzimidazole ring through hydrogen bonding.

First, we checked the catalytic activity of complexes **N1** and **N2**. After that, to confirm the role of the benzimidazolium moiety in the catalytic process, another complex (**N3**) was synthesized with a similar geometry; the only difference was a nonionic bridge instead of the benzimidazolium moiety. Ligand **L2** was synthesized by reacting 2 equiv of 2-mercaptobenzothiazole with 1 equiv of 2,2′-bis-(bromomethyl)-1,1′-biphenyl in dry acetonitrile. The mixture was refluxed for 8 h. After that, the product was separated out as a light-yellow powder and characterized using ^{1}H NMR and ^{13}C NMR (Figures S1−S6). The proton signals due to the methylene group split into two doublets which confirms the formation of the product. Complex **N3** was synthesized by reacting **L2** with copper chloride in methanol and characterized using single crystal X-ray diffraction.

Crystal Structure. Complexes **N1** and **N2** crystallized in a triclinic crystal system with space group $P21/n$, whereas **N3** crystallized in a monoclinic crystal system with space group $P\bar{1}$. The complexes have a copper center with distorted square planar geometry, where halide ions are at trans positions compensating the dipositive charges on the metal ion (Figure 1). In complex **N1**, copper(II) ion is coordinated to dipodal ligand **L1** through nitrogen atoms of the benzimidazole moiety, whereas the other two sites are occupied by halide ions. It is interesting to note that, in complex **N1**, copper perchlorate was used; however, the bromide ions (counterion of **L1**) got coordinated to the copper(II) center. This may be due to the stronger binding affinity of copper ion toward bromide than perchlorate in the particular complex (**N1**) or the conducive geometrical constrains that favors the coordination of bromide ion to the metal center. Also, one of the coordinated bromide ions is interacting with the benzimidazolium moiety through hydrogen bonding, which slightly weakens its coordination with copper ion comparative to another bromide which is evident from the Cu−Br bond distances (Table S2). In complex **N2**, two chloride ions and one ligand **L1** are completing the coordination sphere of Cu(II), whereas one chloride ion is present as a counterion. Similar to complexes **N1** and **N2**, complex **N3** also has a distorted square planar geometry. The structure analyses have revealed that, in complexes **N1** and **N2**, crystal lattices are stabilized by the interplay of hydrogen bonding interaction of the type N−H···O/Cl, C−H···O, and O−H···Cl (hydrogen bonding parameters are given in Tables S5 and S6). No significant hydrogen bonding is observed in complex **N3**, and this may be one of the reasons for poor solubility of **N3** in water. The final R values along with selected refinement details and bond parameters are given in Tables S1−S6. The ORTEP diagrams together with the atom numbering scheme of compounds **N1**−**N3** with 40% probability thermal ellipsoids are shown in Figures S24−S26.

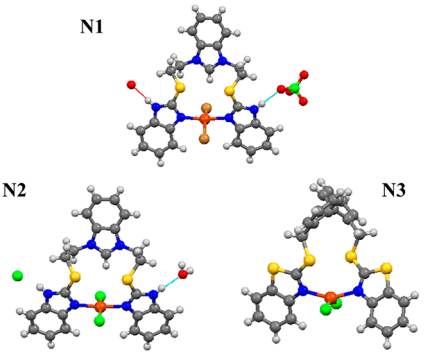

Figure 1. Single crystal structure of copper complexes **N1**, **N2**, and **N3**, showing intramolecular hydrogen bonding.

Photophysical Properties of Copper Complexes. The UV−visible absorbance spectra of ligand **L1**, recorded in an aqueous medium (pH = 8), show two absorbance bands at 248

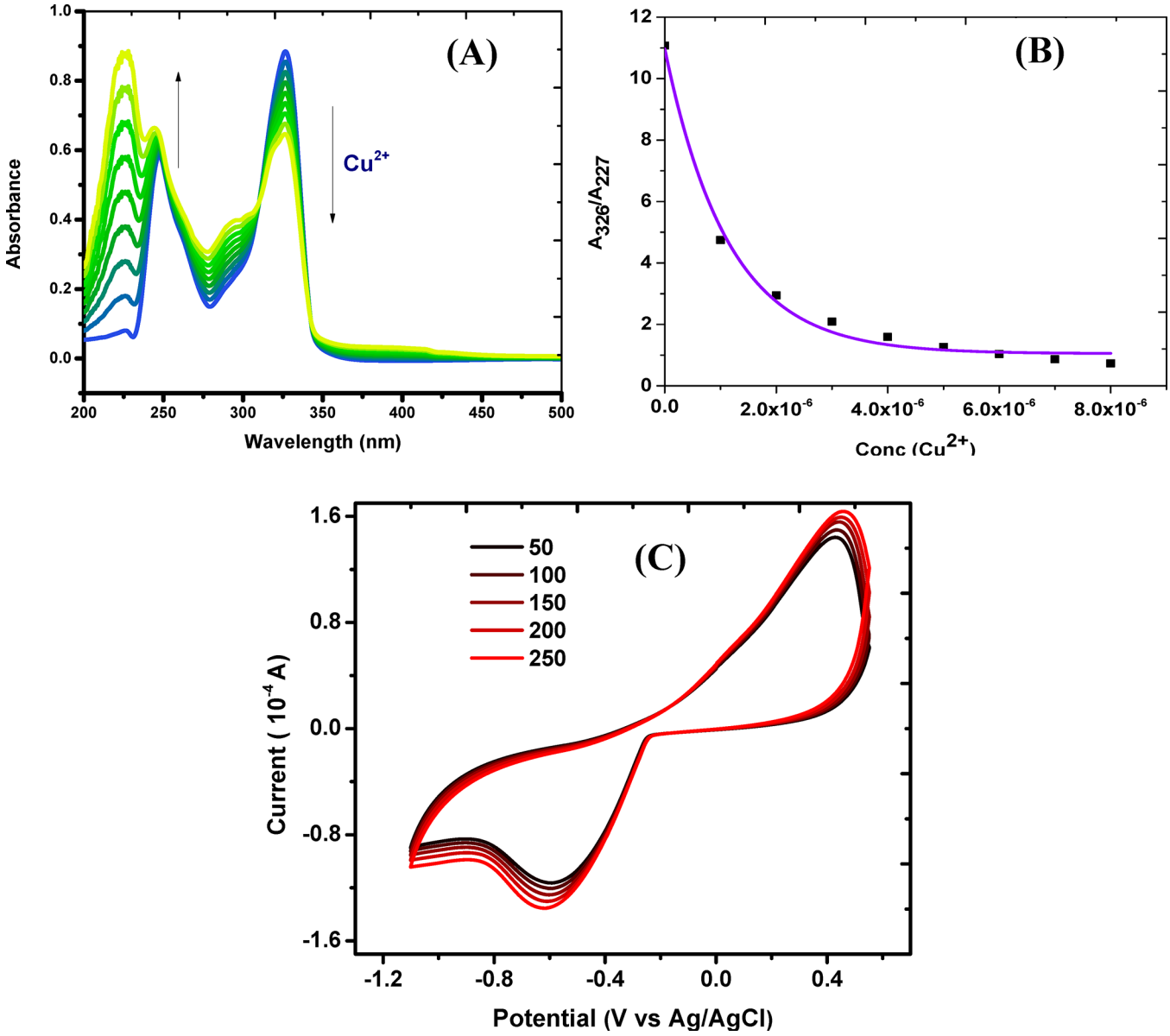

Figure 2. (A) Change in the UV−visible absorption spectra of ligand **L1** (pH = 8.0) upon successive addition of copper chloride (0−8 μM). (B) The nonlinear relationship between the copper ion concentration and absorbance ratio (A_{326}/A_{227}). (C) Cyclic voltammetry profile of complex **N2** (10 μM) at different scan rates.

and 325 nm, respectively, for $\pi-\pi^*$ and n$-\pi^*$ transitions (Figure S7). The successive addition of copper perchlorate to the solution of **L1** leads to a significant change in the absorbance spectra (Figure S8). The absorbance intensity at 248 nm ($\pi-\pi^*$ transition) increases, whereas the absorbance at 325 nm (n$-\pi^*$ transition) decreases. Moreover, a new band at 380 nm appears due to charge transfer between the ligand to metal ion. Similarly, absorbance spectra of **L1** were logged by sequential addition of copper chloride. The absorbance intensity due to the n$-\pi^*$ transition at 326 nm decreases, whereas absorbance maxima corresponding to the $\pi-\pi^*$ transition showed enhancement in intensity. It is worth to remark here that the charge transfer band at 380 nm causes a small enhancement in absorbance intensity, which revealed the poor charge transfer ability of complex **N2** in comparison to that of complex **N1** (Figure 2). The fluorescence spectra of ligands **L1** and **L2** have been recorded in the same solvent system as used for UV−visible absorption spectroscopy. Ligand **L1** was showing strong emission at 405 nm (λ_{ex} = 325 nm), which was quenched by addition of copper perchlorate and copper bromide. However, both complexes **N1** and **N2** were showing a similar behavior in the absorbance profile. Emission intensity of both complexes is almost similar. At the same concentration of copper salt, complex **N1** showed a similar behavior toward fluorescence quenching as the **N2** complex (Figure S11). Complex **N2** has shown weaker charge transfer transition as compared to **N1** that was attributed to a comparatively stronger LMCT (ligand to metal charge transfer) in the **N1** complex.

Due to insolubility of ligand **L2** in water, photophysical studies were carried out in DMSO:water (30:70). Like ligand **L1**, it also shows two absorbance bands at 240 and 315 nm, respectively, due to $\pi-\pi^*$ and n$-\pi^*$ transitions (Table 1). Titration was performed by consecutive addition of copper chloride to **L2** solution (Figures S12 and S13). It was found that copper ions significantly change the absorbance profile of

Table 1. Photophysical Properties of Metal Complexes and Ligands

	λ_{abs} (nm)	λ_{em} (nm)	λ_{ex} (nm)
L1	248, 325	405	248
L2	240, 315	390	240
N1	248, 325, 380	405	248
N2	248, 325, 380	405	248
N3	240, 315, 380	390	240

ligand **L2**. The absorbance intensity at 240 nm increases, whereas, at 315 nm, it decreases, and a new weak band appears at 380 nm due to the weak charge transfer transition. The emission profile of ligand **L2** was recorded at an excitation wavelength of 315 nm which exhibited emission maxima at 390 nm (Figure S14). Fluorescence intensity got quenched as the concentration of copper ions increased. The nonlinear regression between copper ion concentration and emission intensity at 390 nm is showing a linear decrease in fluorescence intensity (Figure S15). This decrease in fluorescence can be explained based on the open shell effect of copper ion.

Electrochemical Studies. The electrochemical studies of prepared complexes were carried out using cyclic voltammetry. The current was measured by varying the potential in the range from 0.55 to −1.1 V. The electrochemical measurements for complexes **N1** and **N2** were recorded at a constant pH of 8.0 in water, whereas, due to the insolubility of complex **N3** in water, studies were carried out in DMSO:water (30:70). Complex **N1** was showing a cathodic peak at 0.43 V, whereas the anodic peak was observed at −0.60 V (Figure S16). To further investigate the electrochemical process, the cyclic voltammetry graph was recorded by varying the scan rate from 50 to 250 mV s^{-1}. The ratio of cathodic and anodic current (I_{pc}/I_{pa}) was greater than 1, which revealed that the process was quasi-reversible. Moreover, that ΔE_p increases with the increase in scan rate also validates the observation. Coulometric experiment by potentiometeric exhaustive electrolysis revealed the consumption of one electron in the redox couple of all the copper complexes. Similarly, electrochemical measurement of complex **N2** discovered the redox process as quasi-reversible. However, complex **N2** showed a comparatively lower value of current for the same concentration (Figure 2), which might be due to more ionic strength of perchlorate ion as compared to bromide ion. The one electron quasi-reversible reduction of the complexes has attributed to the Cu^{+2}/Cu^{+} redox couple. Similarly, redox parameters for complex **N3** were determined as listed in Table 2 (Figure S17).

Table 2. Result of Electrochemical Measurements of Copper Complexes

S. no.	metal complex	E_{pc} (V)	E_{pa} (V)	$E_{1/2}$ (V)	ΔE (mV)
1	**N1**	0.32	−0.60	−0.14	920
2	**N2**	0.43	−0.60	−0.08	1030
3	**N3**	0.47	−0.84	−0.18	1310

Degradation of Phosphorothioate Using N1, N2, and N3 Copper Complexes. The transition metal complexes are known for their phosphatase activity.[61−64] However, few pincer ligand based complexes are reported for detoxification of pesticides. In our previous studies, it is clear that the benzimidazolium ring plays a significant role in detoxification of organophoshates. Therefore, to increase the catalytic efficiency of the benzimidazolium based catalyst, we synthesized their copper complexes. Particularly, copper ion was chosen due to its biocompatibility and affinity to interact with phosphates. To probe the efficiency of our catalyst for the catalytic destruction of the phosphate ester bond, we investigated the ability of the catalyst to degrade the OPs. Ten equivalents of tested organophosphates was added to the 10 μM solution of complex **N1**. The mixture was stirred for 20 min, and after every 2 min, samples were collected for recording the UV−visible absorption spectra. The increase in absorbance intensity at 402 nm can be used to determine the rate of hydrolysis. This enhancement in absorbance intensity is due to release of *para*-nitrophenol. In the case of parathion and paraoxon, the lone pair of electrons on phenolic oxygen shifted toward phosphorus, whereas, upon hydrolysis, the *para*-nitrophenol will release, which results in delocalization of the electron pair inside the aromatic ring; consequently, the absorbance at 402 nm increases.[63] Also, background reactions were carried out without using a catalyst under identical conditions.

As indicated in Figure 3, the plot of time dependent absorbance at 402 nm shows enhancement. Absorbance increased up to 20 min; after that, it becomes constant, which suggests that hydrolysis occurred within 20 min. Furthermore, the effect of substrate concentration on the rate of hydrolysis using the copper complexes as catalyst was investigated by the Michaelis−Menten method (Figure S20). The graph of concentration of substrate vs rate of hydrolysis showed the linear increase up to the concentration of 400 μM, whereas, at higher concentrations, the curve attained saturation that indicated the formation of complex−phosphate intermediates. To calculate the efficiency of the catalysts, a Lineweaver−Burk plot has been constructed (Figure S21). The plot between the inverse of pesticide concentration and inverse of rate shows a linear increase. The Michaelis constants K_M and V_{max} have been calculated for intercept of the Lineweaver−Burk plot and are listed in Table 3. Among all the metal complexes, complex **N2** shows a better catalytic efficiency, whereas complex **N3** has poor catalytic efficiency, suggesting involvement of an ionic benzimidazolium unit in the catalytic process. Therefore, it is a kind of dual catalytic system, made up from organocatalyst and metal ion. Similarly, we have calculated the rate parameters for hydrolysis of different pesticides using complex **N2**, which showed a similar trend for paraoxon, parathion, and methyl-parathion. The effect of pH on the hydrolysis process was also monitored, which indicated that maximum catalytic efficiency was achieved at pH 8, while, in acidic condition, catalytic efficiency decreased (Figures S22 and S23). Moreover, the catalytic efficiency of **N2** is slightly better than that of **N1**, which indicated that complex **N2** may have a greater affinity to interact with organophosphate species in the reversible pathway.

The kinetics parameters for catalyst **N2**, for hydrolysis of different pesticides such as parathion, paraoxon, and methyl-parathion as shown in Table 3, reveal that phosphorothioate pesticides are hydrolyzed with a higher rate than paraoxon. This can be explained on the basis of the higher affinity of sulfur to coordinate with copper ion, which enhances the efficiency of a catalyst. Moreover, the catalytic activity of previously reported catalysts has been compared with the current work which shows an advantage over previous work in terms of high k_{cat} and aqueous solubility.[55,62,65−74]

DOI: 10.1021/acs.inorgchem.9b00779

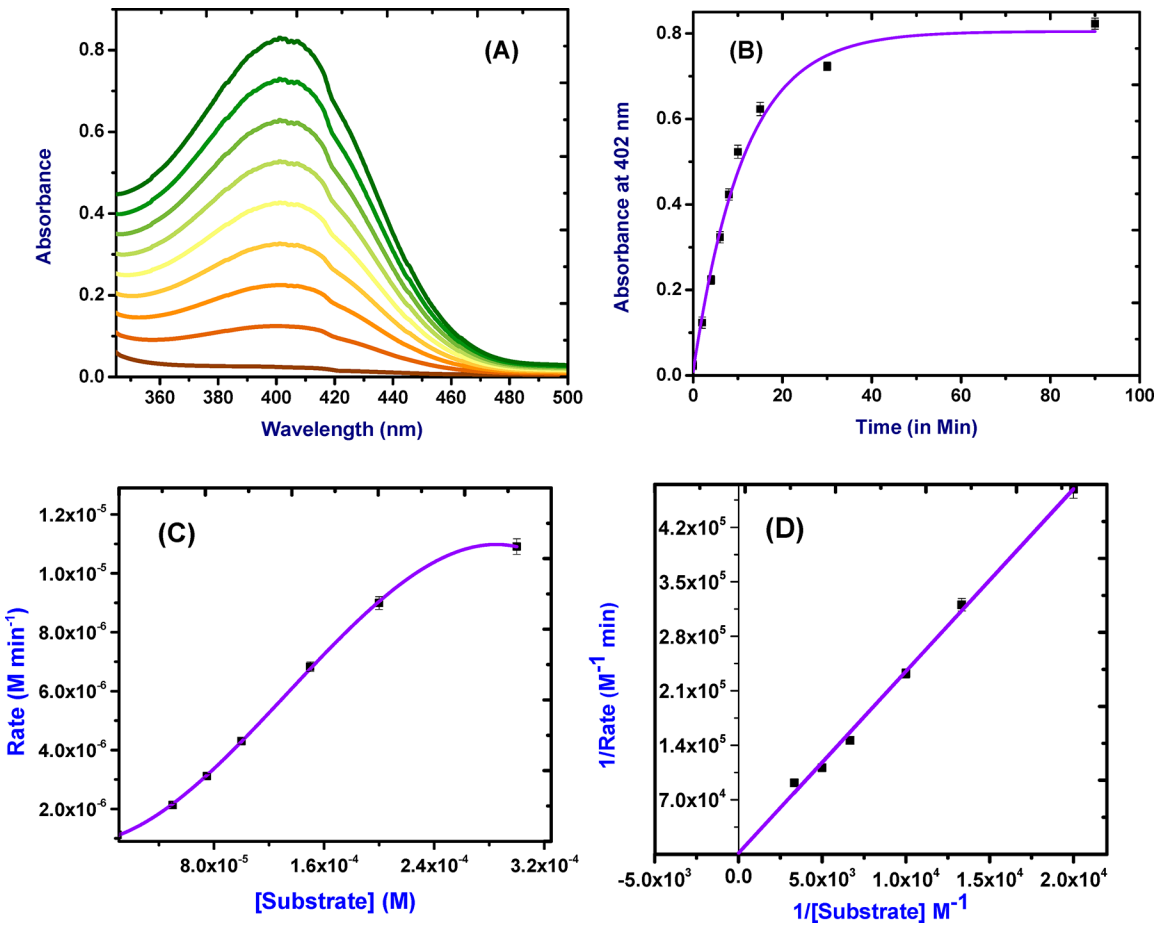

Figure 3. (A) Change in absorbance spectra on conversion of parathion to *para*-nitrophenol using catalyst **N2**. (B) Change in absorbance intensity at 402 nm with the progress of the degradation process. (C) Enzymatic kinetic plot. (D) Lineweaver–Burk plot.

Table 3. First-Order Rate Parameters for Hydrolysis of Different Pesticides As Obtained by the Michaelis–Menten Treatment of Complexes[a]

pesticides	complex	V_{max} (M s^{-1})	K_m (M)	k_{cat} (s^{-1})	k_{cat}/K_m (M^{-1} s^{-1})
parathion	**N1**	5.4×10^{-5}	9.99×10^{-2}	5.45 ± 0.02	54.6 ± 0.18
	N2	6.6×10^{-5}	9.43×10^{-2}	6.67 ± 0.04	70.7 ± 0.21
	N3	9.3×10^{-6}	1.01×10^{-1}	0.93 ± 0.08	9.2 ± 0.10
paraoxon	**N1**	5.3×10^{-5}	1.07×10^{-1}	5.33 ± 0.03	49.6 ± 0.17
	N2	6.2×10^{-5}	9.32×10^{-2}	6.20 ± 0.05	66.5 ± 0.20
	N3	9.4×10^{-6}	9.92×10^{-2}	0.94 ± 0.07	9.4 ± 0.10
methyl-parathion	**N1**	5.3×10^{-5}	1.02×10^{-1}	5.38 ± 0.03	52.7 ± 0.17
	N2	6.4×10^{-5}	9.30×10^{-2}	6.49 ± 0.06	70.1 ± 0.19
	N3	9.2×10^{-6}	1.05×10^{-1}	0.92 ± 0.09	8.7 ± 0.09

[a]Note: All the experiments were repeated three times, and the average value of data has been taken to calculate the catalytic parameter.

^{31}P NMR spectra were used to investigate the mechanism of hydrolysis reaction of methyl-parathion in the presence of catalyst **N2** (Figure S27A). ^{31}P NMR spectra obtained in the successive time periods of reaction exhibit two species: the signal at δ = 65.46 ppm corresponds to methyl-parathion which is slightly upfield shifted (δ = 63.58 ppm) in the presence of **N2** catalyst. The signal at δ = 63.58 ppm disappears during the reaction, and a new signal at δ = 61.80 ppm appears which can be assigned to the hydrolyzed product, dimethyl thiohydrogen phosphate [$(CH_3O)_2(OH)P{=}S$].[75,76] Furthermore, the photographic images of the hydrolysis reaction were recorded with regular intervals of time as in Figure S27B. The investigation reveals that the colorless solution of methyl-parathion was changed to yellow after 25 min, which is attributed to the formation of *para*-nitrophenol. Therefore, it can be predicted that methyl-parathion is hydrolyzed into dimethyl thiophosphate and *para*-nitrophenol.

Plausible Mechanism of Degradation. As shown in the crystal structure of complex **N1**, copper is in a distorted square planar geometry, with two bromide ions covalently attached to a copper ion. It is worth to mention that both bromide ions are not in the same coordination with the copper ion. One of the bromide ions is interacting with benzimidazolium hydrogen through hydrogen bonding. The organophosphate can occupy the fifth coordination site of copper ion through the reversible pathway, in such a way that acidic hydrogen of the

DOI: 10.1021/acs.inorgchem.9b00779

Scheme 3. Plausible Mechanism of Degradation of Organophosphate Based Pesticides

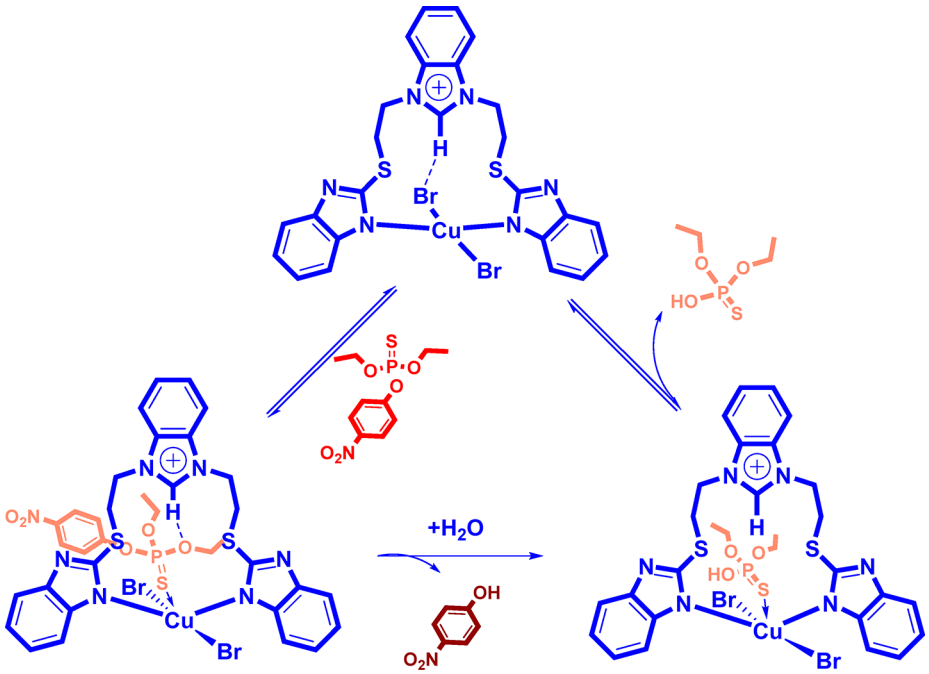

benzimidazolium cation can interact with organophosphate through hydrogen bonding (Scheme 3). Both of these interactions enhance the electrophilicity of the phosphorus center and therefore will enhance the rate of hydrolysis.[66] Here, two catalytic centers (benzimidazolium as organocatalyst and copper ion as metal based catalyst) work synergistically to enhance the catalytic activity for hydrolysis of pesticides. To investigate further the role of the benzimidazolium moiety in the catalytic process, an additional metal complex (**N3**) was prepared with a similar binding environment for copper ion; however, the nonionic biphenyl ring replaced the benzimidazolium ring. The prepared copper complex of the nonionic ligand was also explored for degradation of pesticides; however, it showed a negligible activity in comparison to that of complex **N1**. Moreover, the ability of ligand **L1** for the hydrolysis of pesticide was examined, which revealed that it did not catalyze the hydrolysis of the pesticide (Table S9).

Supramolecular interactions involved in the solid state structure were investigated further to determine the mechanism of degradation of organophosphates (Figure 4).

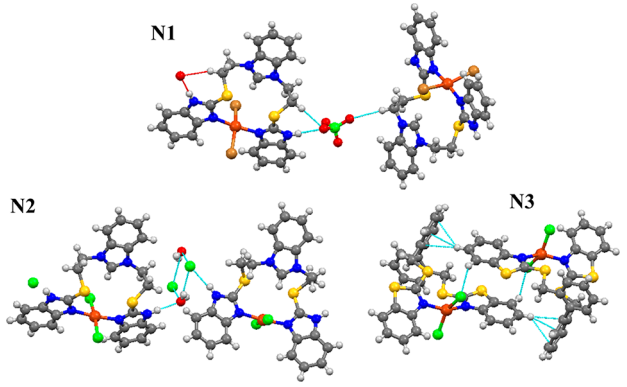

Figure 4. Noncovalent interactions involved in supramolecular packing of complexes **N1**, **N2**, and **N3**.

Although, we have carried out all catalytic studies in the solution phase, but these noncovalent interactions play an important role in the catalytic activity of complexes.[66] It was revealed from the solid state structure analyses that, in complex **N2**, a water molecule interacts with the benzimidazole hydrogen (N-H) and chloride ion through hydrogen bonding, which enhances the nucleophilicity of water toward the nucleophilic substitution reaction at the phosphorus center. Histidine plays a catalytic role in various enzymatic reactions by interacting with nucleophilic species through hydrogen bonding.[39] Therefore, it is believed that noncovalent interactions are responsible for the catalytic activity of complexes in the present study. In complex **N1**, a similar type of hydrogen bonding interaction is observed with water molecules and perchlorate ions. Due to the absence of any counterion in complex **N3**, hydrogen bonding with a solvent molecule and anion is absent. Although, other interactions, such as C−H···Cl and C−H···π, are involved in supramolecular packing of investigated complexes. These interactions do not affect the catalytic activity of complexes; thus the absence of such a kind of interaction in complex **N3** could be another reason for the lack of a catalytic affinity toward the hydrolysis of organophosphate species.

Quantitative Investigation of Acetylcholine Esterase Activity. Quantitative investigation of acetylcholine esterase activity has been demonstrated using Ellman's assay which makes use of Ellman's reagent (dithiobisnitro-benzoate, DTNB), a highly reactive reagent having a S−S bond that breaks quickly by reacting with a free thiol group and gives the intense yellow color of thiobisnitro-benzoate ion (Scheme 4). In this way, hydrolysis of acetylthiocholine into thiocholine could be monitored using Ellman's assay by measuring the characteristic absorption band at λ_{max} = 412 nm due to generation of a thiobisnitro-benzoate ion.[29,77] Because parathion will cause interference due to its byproduct (*para*-nitrophenol), we used diethyl chlorophosphate as a pesticide that has a similar reactivity as parathion and releases byproduct

DOI: 10.1021/acs.inorgchem.9b00779

Scheme 4. Complete Scheme for Colorimetric Determination of Cholinesterase Activities: Ellman's Assay

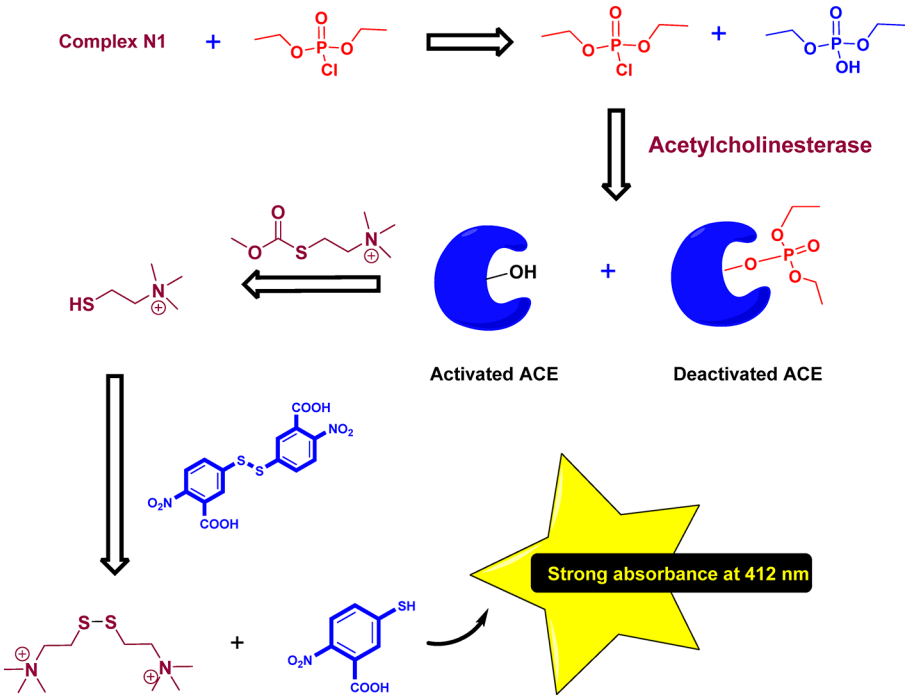

that did not cause any interference in region 412 nm. Diethyl chlorophosphate (100 μM) reacted with complex **N1** (10 μM) for 20 min; after every 2 min, the sample was collected from the reaction mixture. To the collected sample (80 μL) was added a solution of acetylcholine esterase enzyme, followed by addition of Ellman solution (10 μL). All the collected samples were put in a 96-well plate, and the absorbance intensity at 412 nm was recorded using a TECAN plate reader.

The increase in absorbance at 412 nm is attributed to the free thiol group in the solution and was used to monitor the hydrolysis of acetylthiocholine. It was observed that, in the presence of a catalyst, the concentration of free thiol decreases up to 13% within 20 min (Figure 5). Therefore, our catalyst is efficient toward detoxification of organophosphates in a very short span of time. It is worth to be mentioned here that **N2** complex also effectively decreases the inhibition of acetylcholine esterase enzyme in the presence of organophosphate, whereas complex **N3** was not found to be effective to reduce the inhibition of enzyme (Figures S28 and S29).

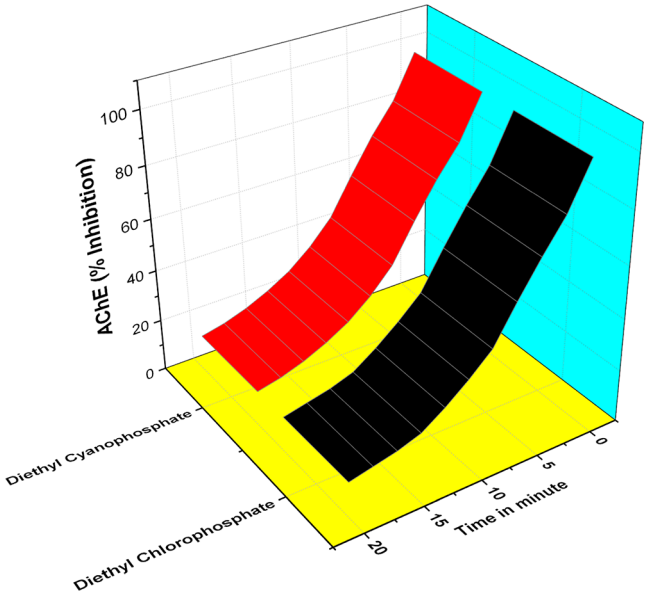

Figure 5. Detoxification of diethyl chlorophosphate and diethyl cyanophosphate by complex **N2**. Data are given as the mean of two assays.

CONCLUSION

We have synthesized novel copper(II) complexes having a benzimidazolium unit as a secondary catalytic site along with the primary catalytic site of copper ion. Complexes **N1** and **N2** coordinate with organophosphate species in a reversible pathway, which enhances the electrophilicity of phosphorus and favors the hydrolysis process. The rate of hydrolysis of first-order kinetics was measured using UV−visible absorption spectroscopy by monitoring the absorption at 405 nm. The prepared catalyst has various advantages over existing methods, such as a high rate of hydrolysis, working in the pure aqueous medium, and a better catalytic efficiency. To demonstrate further the acetylcholine esterase activity, Ellman's reagent was used to monitor the hydrolysis of acetylthiocholine. The inhibition of acetylcholine esterase enzyme due to pesticide decreased up to 13% within 20 min.

ASSOCIATED CONTENT

Supporting Information

The Supporting Information is available free of charge on the ACS Publications website at DOI: 10.1021/acs.inorgchem.9b00770.

UV−visible absorption, emission, ^{1}H NMR, ^{13}C NMR, bond angles, and bond length of complexes (PDF)

Accession Codes

CCDC 1818792−1818794 contain the supplementary crystallographic data for this paper. These data can be obtained free of charge via www.ccdc.cam.ac.uk/data_request/cif, or by

emailing data_request@ccdc.cam.ac.uk, or by contacting The Cambridge Crystallographic Data Centre, 12 Union Road, Cambridge CB2 1EZ, UK; fax: +44 1223 336033.

■ AUTHOR INFORMATION

Corresponding Authors

*E-mail: nsingh@iitrpr.ac.in. Tel: +91-1881242176 (N.S.).
*E-mail: navneetkaur@pu.ac.in. Phone: +91 9815245098 (N.K.).

ORCID

Amanpreet Singh: 0000-0002-1461-4607
Jan J. Dubowski: 0000-0003-0022-527X
Narinder Singh: 0000-0002-8794-8157

Notes

The authors declare no competing financial interest.

■ ACKNOWLEDGMENTS

This work was supported by a research grant from the joint Indo-Canada project sponsored by DBT-New Delhi and IC-IMPACTS Canada. A.S. and P.R. are thankful to the Indian Institute of Technology, Ropar, for the Director-postdoc fellowship.

■ REFERENCES

(1) Kim, K.; Tsay, O. G.; Atwood, D. A.; Churchill, D. G. Destruction and Detection of Chemical Warfare Agents. *Chem. Rev.* **2011**, *111*, 5345−5403.

(2) Singh, A.; Raj, P.; Singh, N. Benzimidazolium-Based Self-Assembled Fluorescent Aggregates for Sensing and Catalytic Degradation of Diethylchlorophosphate. *ACS Appl. Mater. Interfaces* **2016**, *8*, 28641−28651.

(3) Sambrook, M. R.; Hiscock, J. R.; Cook, A.; Green, a C.; Holden, I.; Vincent, J. C.; Gale, P. A. Hydrogen Bond-Mediated Recognition of the Chemical Warfare Agent Soman (GD). *Chem. Commun.* **2012**, *48*, 5605−5607.

(4) Yao, J.; Fu, Y.; Xu, W.; Fan, T.; Gao, Y.; He, Q.; Zhu, D.; Cao, H.; Cheng, J. Concise and Efficient Fluorescent Probe via an Intromolecular Charge Transfer for the Chemical Warfare Agent Mimic Diethylchlorophosphate Vapor Detection. *Anal. Chem.* **2016**, *88*, 2497−2501.

(5) Klet, R. C.; Liu, Y.; Wang, T. C.; Hupp, T.; Farha, O. K. Evaluation of Brønsted Acidity and Proton Topology in Zr- and Hf-Based Metal−organic Frameworks Using Potentiometric Acid−base Titration. *J. Mater. Chem. A* **2016**, *4*, 1479−1485.

(6) Le, Q. A. T.; Chang, R.; Kim, Y. H. Rational Design of Paraoxonase 1 (PON1) for the Efficient Hydrolysis of Organophosphates. *Chem. Commun.* **2015**, *51*, 14536−14539.

(7) Diaz de Grenu, B.; Moreno, D.; Torroba, T.; Berg, A.; Gunnars, J.; Nilsson, T.; Nyman, R.; Persson, M.; Pettersson, J.; Eklind, I.; Wasterby, P. Fluorescent Discrimination between Traces of Chemical Warfare Agents and Their Mimics. *J. Am. Chem. Soc.* **2014**, *136*, 4125−4128.

(8) Bhat, G. A.; Maqbool, R.; Dar, A. A.; Ul Hussain, M.; Murugavel, R. Selective Formation of Discrete versus Polymeric Copper Organophosphates: DNA Cleavage and Cytotoxic Activity. *Dalt. Trans.* **2017**, *46*, 13409−13420.

(9) Viveros, L.; Paliwal, S.; McCrae, D.; Wild, J.; Simonian, A. A Fluorescence-Based Biosensor for the Detection of Organophosphate Pesticides and Chemical Warfare Agents. *Sens. Actuators, B* **2006**, *115*, 150−157.

(10) Mondloch, J. E.; Katz, M. J.; Isley, W. C., III; Ghosh, P.; Liao, P.; Bury, W.; Wagner, G. W.; Hall, M. G.; Decoste, J. B.; Peterson, G. W.; Snurr, R. Q.; Cramer, C. J.; Hupp, J. T.; Farha, O. K. Destruction of Chemical Warfare Agents Using Metal−organic Frameworks. *Nat. Mater.* **2015**, *14*, 512−516.

(11) Lum, K. T.; Huebner, H. J.; Li, Y.; Phillips, T. D.; Raushel, F. M. Organophosphate Nerve Agent Toxicity in Hydra Attenuata. *Chem. Res. Toxicol.* **2003**, *16*, 953−957.

(12) Liu, Y.; Bonizzoni, M. A Supramolecular Sensing Array for Qualitative and Quantitative Analysis of Organophosphates in Water. *J. Am. Chem. Soc.* **2014**, *136*, 14223−14229.

(13) Totten, R. K.; Kim, Y. S.; Weston, M. H.; Farha, O. K.; Hupp, J. T.; Nguyen, S. T. Enhanced Catalytic Activity through the Tuning of Micropore Environment and Supercritical CO_2 Processing: Al-(Porphyrin)-Based Porous Organic Polymers for the Degradation of a Nerve Agent Simulant. *J. Am. Chem. Soc.* **2013**, *135*, 11720−11723.

(14) Pinto, G.; Mazzone, G.; Russo, N.; Toscano, M. Trimethylphosphate and Dimethylphosphate Hydrolysis by Binuclear Cd^{II}, Mn^{II}, and Zn^{II} − Fe^{II} Promiscuous Organophosphate- Degrading Enzyme : Reaction Mechanisms. *Chem. - Eur. J.* **2017**, *23*, 13742−13753.

(15) Moon, S.; Proussaloglou, E.; Peterson, G. W.; Decoste, J. B.; Hall, M. G.; Howarth, A. J.; Hupp, J. T.; Farha, O. K. Detoxification of Chemical Warfare Agents Using a Zr 6 -Based Metal − Organic Framework/Polymer Mixture. *Chem. - Eur. J.* **2016**, *22*, 14864−14868.

(16) Woo, D. J.; Obendorf, S. K. MgO-Embedded Fibre-Based Substrate as an Effective Sorbent for Toxic Organophosphates. *RSC Adv.* **2014**, *4*, 15727.

(17) Braatz, A. D.; Antonio, M. R.; Nilsson, M. Structural Study of Complexes Formed by Acidic and Neutral Organophosphorus Reagents. *Dalt. Trans.* **2017**, *46*, 1194−1206.

(18) Gupta, S. K.; Dar, A. A.; Rajeshkumar, T.; Kuppuswamy, S.; Langley, S. K.; Murray, K. S.; Rajaraman, G.; Murugavel, R. Discrete $\{Gd^{III}{}_4M\}$ (M = Gd^{III} or Co^{II}) Pentanuclear Complexes: A New Class of Metal-Organophosphate Molecular Coolers. *Dalt. Trans.* **2015**, *44*, 5961−5965.

(19) Singh, A. K.; Flounders, A. W.; Volponi, J. V.; Ashley, C. S.; Wally, K.; Schoeniger, J. S. Development of Sensors for Direct Detection of Organophosphates. Part I: Immobilization, Characterization and Stabilization of Acetylcholinesterase and Organophosphate Hydrolase on Silica Supports. *Biosens. Bioelectron.* **1999**, *14*, 703−713.

(20) Liu, G.; Lin, Y. Biosensor Based on Self-Assembling Acetylcholinesterase on Carbon Nanotubes for Flow Injection/amperometric Detection of Organophosphate Pesticides and Nerve Agents. *Anal. Chem.* **2006**, *78*, 835−843.

(21) Tormos, J. R.; Wiley, K. L.; Wang, Y.; Fournier, D.; Masson, P.; Nachon, F.; Quinn, D. M. Accumulation of Tetrahedral Intermediates in Cholinesterase Catalysis: A Secondary Isotope Effect Study. *J. Am. Chem. Soc.* **2010**, *132*, 17751−17759.

(22) Liu, D.; Chen, W.; Wei, J.; Li, X.; Wang, Z.; Jiang, X. A Highly Sensitive, Dual-Readout Assay Based on Gold Nanoparticles for Organophosphorus and Carbamate Pesticides. *Anal. Chem.* **2012**, *84*, 4185−4191.

(23) Fenzl, C.; Genslein, C.; Zöpfl, A.; Baeumner, A. J.; Hirsch, T. A Photonic Crystal Based Sensing Scheme for Acetylcholine and Acetylcholinesterase Inhibitors. *J. Mater. Chem. B* **2015**, *3*, 2089−2095.

(24) Qian, S.; Lin, H. Colorimetric Sensor Array for Detection and Identification of Organophosphorus and Carbamate Pesticides. *Anal. Chem.* **2015**, *87*, 5395−5400.

(25) Zhu, X.; Li, B.; Yang, J.; Li, Y.; Zhao, W.; Shi, J.; Gu, J. Effective Adsorption and Enhanced Removal of Organophosphorus Pesticides from Aqueous Solution by Zr-Based MOFs of UiO-67. *ACS Appl. Mater. Interfaces* **2015**, *7*, 223−231.

(26) Li, H.; Li, J.; Xu, Q.; Hu, X. Poly(3-hexylthiophene)/TiO_2 Nanoparticle-Functionalized Electrodes for Visible Light and Low Potential Photoelectrochemical Sensing of Organophosphorus Pesticide Chlopyrifos. *Anal. Chem.* **2011**, *83*, 9681−9686.

(27) de Koning, M. C.; Joosen, M. J. A.; Worek, F.; Nachon, F.; van Grol, M.; Klaassen, S. D.; Alkema, D. P. W.; Wille, T.; de Bruijn, H. M. Application of the Ugi Multicomponent Reaction in the Synthesis

of Reactivators of Nerve Agent Inhibited Acetylcholinesterase. *J. Med. Chem.* **2017**, *60*, 9376−9392.
(28) Liao, S.; Han, W.; Ding, H.; Xie, D.; Tan, H.; Yang, S.; Wu, Z.; Shen, G.; Yu, R. Modulated Dye Retention for the Signal-on Fluorometric Determination of Acetylcholinesterase Inhibitor. *Anal. Chem.* **2013**, *85*, 4968−4973.
(29) Lei, C.; Wang, Z.; Nie, Z.; Deng, H.; Hu, H.; Huang, Y.; Yao, S. Resurfaced Fluorescent Protein as a Sensing Platform for Label-Free Detection of copper(II) Ion and Acetylcholinesterase Activity. *Anal. Chem.* **2015**, *87*, 1974−1980.
(30) Purohit, C. S.; Mishra, A. K.; Verma, S. Four-Stranded Coordination Helices Containing Silver−Adenine (Purine) Metallaquartets. *Inorg. Chem.* **2007**, *46*, 8493−8495.
(31) Mishra, A. K.; Verma, S. Interconnected Trimeric, Pentameric, and Hexameric Metallacycles in a Singular Silver - Adenine Framework. *Inorg. Chem.* **2010**, *49*, 8012−8016.
(32) Pandey, M. D.; Mishra, A. K.; Chandrasekhar, V.; Verma, S. Silver-Guided Excimer Emission in an Adenine - Pyrene Conjugate : Fluorescence Lifetime and Crystal Studies. *Inorg. Chem.* **2010**, *49*, 2020−2022.
(33) Hadler, K. S.; Mitic, N.; Yip, S. H.-C.; Gahan, L. R; Ollis, D. L.; Schenk, G.; Larrabee, J. A. Electronic Structure Analysis of the Dinuclear Metal Center in the Bioremediator Glycerophosphodiesterase (GpdQ) from Enterobacter Aerogenes. *Inorg. Chem.* **2010**, *48*, 2727−2734.
(34) Hadler, K. S.; Tanifum, E. A.; Yip, S. H.-C.; Mitic, N.; Guddat, L. W.; Jackson, C. J.; Gahan, L. R.; Nguyen, K.; Carr, P. D.; Ollis, D. L.; Hengge, A. C.; Larrabee, J. A.; Schenk, G. Substrate-Promoted Formation of a Catalytically Competent Binuclear Center and Regulation of Reactivity in a Glycerophosphodiesterase from Enterobacter Aerogenes. *J. Am. Chem. Soc.* **2008**, *130*, 14129−14138.
(35) Pedroso, M. M.; Ely, F.; Mitic, N.; Carpenter, M. C.; Gahan, L. R.; Wilcox, D. E.; Larrabee, J. L.; Ollis, D. L.; Schenk, G. Comparative Investigation of the Reaction Mechanisms of the Organophosphate-Degrading Phosphotriesterases from Agrobacterium Radiobacter (OpdA) and Pseudomonas Diminuta (OPH). *J. Biol. Inorg. Chem.* **2014**, *19*, 1263−1275.
(36) Ng, T.; Gahan, L. R.; Schenk, G.; Ollis, D. L. Altering the Substrate Specificity of Methyl Parathion Hydrolase with Directed Evolution. *Arch. Biochem. Biophys.* **2015**, *573*, 59−68.
(37) Schenk, G.; Mateen, I.; Ng, T.-K.; Pedroso, M. M.; Mitic, N.; Jafelicci, M.; Marques, R. F.C.; Gahan, L. R.; Ollis, D. L. Organophosphate-Degrading Metallohydrolases : Structure and Function of Potent Catalysts for Applications in Bioremediation. *Coord. Chem. Rev.* **2016**, *317*, 122−131.
(38) Hadler, K. S.; Mitic, N.; Ely, F.; Hanson, G. R.; Gahan, L. R; Larrabee, J. A.; Ollis, D. L.; Schenk, G. Structural Flexibility Enhances the Reactivity of the Bioremediator Glycerophosphodiesterase by Fine-Tuning Its Mechanism of Hydrolysis. *J. Am. Chem. Soc.* **2009**, *131*, 11900−11908.
(39) Sharma, U. K.; Sharma, N.; Kumar, R.; Kumar, R.; Sinha, A. K. Biocatalytic Promiscuity of Lipase in Chemoselective Oxidation of Aryl Alcohols/Acetates : A Unique Synergism of CAL-B and [hmim] Br for the Metal-Free H_2O_2 Activation. *Org. Lett.* **2009**, *11*, 4846−4848.
(40) Zhao, Y.; Li, Z.; Sharma, U. K.; Sharma, N.; Song, G.; Van der Eycken, E. V. Copper-Catalyzed Alkylarylation of Activated Alkenes Using Isocyanides as the Alkyl Source : an efficient radical access to 3,3-dialkylated oxindoles. *Chemchomm* **2016**, *52*, 6395−6398.
(41) Sharma, H.; Kaur, N.; Singh, N.; Jang, D. O. Synergetic Catalytic Effect of Ionic Liquids and ZnO Nanoparticles on the Selective Synthesis of 1,2-Disubstituted Benzimidazoles Using a Ball-Milling Technique. *Green Chem.* **2015**, *17*, 4263−4270.
(42) Zhang, Q.; Zhang, S.; Deng, Y. Recent Advances in Ionic Liquid Catalysis. *Green Chem.* **2011**, *13*, 2619−2637.
(43) Mehnert, C. P.; Mozeleski, E. J.; Cook, R. A. Supported Ionic Liquid Catalysis Investigated for Hydrogenation Reactions. *Chem. Commun.* **2002**, *24*, 3010−3011.
(44) Ghosh, A. K.; Brindisi, M. Organic Carbamates in Drug Design and Medicinal Chemistry. *J. Med. Chem.* **2015**, *58*, 2895−2940.
(45) Sit, R. K.; Fokin, V. V.; Amitai, G.; Sharpless, K. B.; Taylor, P.; Radic, Z. Imidazole Aldoximes Effective in Assisting Butyrylcholinesterase Catalysis of Organophosphate Detoxification. *J. Med. Chem.* **2014**, *57*, 1378−1389.
(46) Rajendiran, S.; Park, K.; Lee, K.; Yoon, S. Ionic-Liquid-Based Heterogeneous Covalent Triazine Framework Cobalt Catalyst for the Direct Synthesis of Methyl 3-Hydroxybutyrate from Propylene Oxide. *Inorg. Chem.* **2017**, *56*, 7270−7277.
(47) Pavez, P.; Millan, D.; Morales, J. I.; Castro, E. A.; Lopez A, C.; Santos, J. G. Mechanisms of Degradation of Paraoxon in Different Ionic Liquids. *J. Org. Chem.* **2013**, *78*, 9670−9676.
(48) Totten, R. K.; Weston, M. H.; Park, J. K.; Farha, O. K.; Hupp, J. T.; Nguyen, S. T. Catalytic Solvolytic and Hydrolytic Degradation of Toxic Methyl Paraoxon with La(catecholate)-Functionalized Porous Organic Polymers. *ACS Catal.* **2013**, *3*, 1454−1459.
(49) Bromberg, L.; Creasy, W. R.; McGarvey, D. J.; Wilusz, E.; Hatton, T. A. Nucleophilic Polymers and Gels in Hydrolytic Degradation of Chemical Warfare Agents. *ACS Appl. Mater. Interfaces* **2015**, *7*, 22001−22011.
(50) Islamoglu, T.; Atilgan, A.; Moon, S.-Y.; Peterson, G. W.; DeCoste, J. B.; Hall, M.; Hupp, J. T.; Farha, O. K. Cerium(IV) vs Zirconium(IV) Based Metal−Organic Frameworks for Detoxification of a Nerve Agent. *Chem. Mater.* **2017**, *29*, 2672−2676.
(51) Li, P.; Moon, S. Y.; Guelta, M. A.; Lin, L.; Gomez-Gualdron, D. A.; Snurr, R. Q.; Harvey, S. P.; Hupp, J. T.; Farha, O. K. Nanosizing a Metal-Organic Framework Enzyme Carrier for Accelerating Nerve Agent Hydrolysis. *ACS Nano* **2016**, *10*, 9174−9182.
(52) Singh, A.; Singh, J.; Singh, N.; Jang, D. O. A Benzimidazolium-Based Mixed Organic−inorganic Polymer of Cu(II) Ions for Highly Selective Sensing of Phosphates in Water: Applications for Detection of Harmful Organophosphates. *Tetrahedron* **2015**, *71*, 6143−6147.
(53) Raj, P.; Singh, A.; Kaur, K.; Aree, T.; Singh, A.; Singh, N. Fluorescent Chemosensors for Selective and Sensitive Detection of Phosmet/Chlorpyrifos with Octahedral Ni^{2+} Complexes. *Inorg. Chem.* **2016**, *55*, 4874−4883.
(54) Raj, P.; Singh, A.; Singh, A.; Singh, N. Syntheses, Crystal Structures and Photophysical Properties of Cu(II) Complexes: Fine Tuning of a Coordination Sphere for Selective Binding of Azamethiphos. *Dalt. Trans.* **2017**, *46*, 985−994.
(55) Daumann, L. J.; Schenk, G.; Ollis, D. L.; Gahan, L. R. Spectroscopic and Mechanistic Studies of Dinuclear Metallohydrolases and Their Biomimetic Complexes. *Dalt. Trans.* **2014**, *43*, 910−928.
(56) Sendzik, M.; Pushie, M. J.; Stefaniak, E.; Haas, K. L. Structure and Affinity of Cu(I) Bound to Human Serum Albumin. *Inorg. Chem.* **2017**, *56*, 15057−15065.
(57) Singh, A.; Singh, A.; Singh, N.; Jang, D. O. A Benzimidazolium-Based Organic Trication: A Selective Fluorescent Sensor for Detecting Cysteine in Water. *RSC Adv.* **2015**, *5*, 72084−72089.
(58) Chen, L.; Khadivi, A.; Singh, M.; Jurss, J. W. Synthesis of a Pentadentate, Polypyrazine Ligand and Its Application in Cobalt-Catalyzed Hydrogen Production. *Inorg. Chem. Front.* **2017**, *4*, 1649−1653.
(59) Bauer, G.; Hu, X. Recent Developments of Iron Pincer Complexes for Catalytic Applications. *Inorg. Chem. Front.* **2016**, *3*, 741−765.
(60) DeMott, J. C.; Dekarske, J. R.; McCulloch, B. J.; Ozerov, O. V. Cyclometallation of the NNN Pincer Ligand in Complexes of Platinum. *Inorg. Chem. Front.* **2015**, *2*, 912−916.
(61) Sanyal, R.; Guha, A.; Ghosh, T.; Mondal, T. K.; Zangrando, E.; Das, D. Influence of the Coordination Environment of zinc(II) Complexes of Designed Mannich Ligands on Phosphatase Activity: A Combined Experimental and Theoretical Study. *Inorg. Chem.* **2014**, *53*, 85−96.
(62) Sanyal, R.; Zhang, X.; Kundu, P.; Chattopadhyay, T.; Zhao, C.; Mautner, F. A.; Das, D. Mechanistic Implications in the Phosphatase

Activity of Mannich-Based Dinuclear Zinc Complexes with Theoretical Modeling. *Inorg. Chem.* **2015**, *54*, 2315−2324.

(63) Arora, H.; Barman, S. K.; Lloret, F.; Mukherjee, R. Isostructural Dinuclear Phenoxo-/acetato-Bridged manganese(II), cobalt(II), and zinc(II) Complexes with Labile Sites: Kinetics of Transesterification of 2-Hydroxypropyl-P-Nitrophenylphosphate. *Inorg. Chem.* **2012**, *51*, 5539−5553.

(64) Esteves, L. F.; Rey, N. A.; Dos Santos, H. F.; Costa, L. A. S. Theoretical Proposal for the Whole Phosphate Diester Hydrolysis Mechanism Promoted by a Catalytic Promiscuous Dinuclear Copper(II) Complex. *Inorg. Chem.* **2016**, *55*, 2806−2818.

(65) Osorio, R. E. H. M. B.; Peralta, R. A.; Bortoluzzi, A. J.; de Almeida, V. R.; Szpoganicz, B.; Fischer, F. L.; Terenzi, H.; Mangrich, A. S.; Mantovani, K. M.; Ferreira, D. E. C.; Rocha, W. R.; Haase, W.; Tomkowicz, Z.; Anjos, A. d.; Neves, A. Synthesis, Magnetostructural Correlation, and Catalytic Promiscuity of Unsymmetric Dinuclear Copper(II) Complexes: Models for Catechol Oxidases and Hydrolases. *Inorg. Chem.* **2012**, *51*, 1569−1589.

(66) Camargo, T. P.; Neves, A.; Peralta, R. A.; Chaves, C.; Maia, E. C. P.; Lizarazo-Jaimes, E. H.; Gomes, D. A.; Bortolotto, T.; Norberto, D. R.; Terenzi, H.; Tierney, D. L.; Schenk, G. Second-Sphere Effects in Dinuclear $Fe^{III}Zn^{II}$ Hydrolase Biomimetics: Tuning Binding and Reactivity Properties. *Inorg. Chem.* **2018**, *57*, 187−203.

(67) Osorio, R. E.H.M.B.; Neves, A.; Camargo, T. P.; Mireski, S. L.; Bortoluzzi, A. J.; Castellano, E. E.; Haase, W.; Tomkowicz, Z. Synthesis, Structure, Magnetism, and Hydrolase and Catecholase Activity of a New Trinuclear Copper (II) Complex. *Inorg. Chim. Acta* **2015**, *435*, 153−158.

(68) Peralta, R. A.; Bortoluzzi, A. J.; de Souza, B.; Jovito, R.; Xavier, F. R.; Couto, R. A. A.; Casellato, A.; Nome, F.; Dick, A.; Gahan, L.. R.; Schenk, G.; Hanson, G. R.; de Paula, F. C. S.; Pereira-Maia, E. C.; de P. Machado, S.; Severino, P. C.; Pich, C.; Bortolotto, T.; Terenzi, H.; Castellano, E. E.; Neves, A.; Riley, M. J. Electronic Structure and Spectro-Structural Correlations of $Fe^{III}Zn^{II}$ Biomimetics for Purple Acid Phosphatases : Relevance to DNA Cleavage and Cytotoxic Activity. *Inorg. Chem.* **2010**, *49*, 11421−11438.

(69) dos Santos Silva, G. A.; Amorim, A. L.; Souza, B. d.; Gabriel, P.; Terenzi, H.; Nordlander, E.; Neves, A.; Peralta, R. A. Synthesis and Characterization of FeIII(μ-OH)ZnII Complexes: Effects of a Second Coordination Sphere and Increase in the Chelate Ring Size on the Hydrolysis of a Phosphate Diester and DNA. *Dalt. Trans.* **2017**, *46*, 11380−11394.

(70) Jarenmark, M.; Csapo, E.; Singh, J.; Wockel, S.; Farkas, E.; Meyer, F.; Haukka, M.; Nordlander, E. Unsymmetrical Dizinc Complexes as Models for the Active Sites of Phosphohydrolases. *Dalton Trans.* **2010**, *39*, 8183−8194.

(71) Jarenmark, M.; Haukka, M.; Demeshko, S.; Tuczek, F.; Zuppiroli, L.; Meyer, F.; Nordlander, E. Synthesis, Characterization, and Reactivity Studies of Heterodinuclear Complexes Modeling Active Sites in Purple Acid Phospatases. *Inorg. Chem.* **2011**, *50*, 3866−3887.

(72) Roberts, A. E.; Schenk, G.; Gahan, L. R. A Heterodinuclear Fe III Zn II Complex as a Mimic for Purple Acid Phosphatase with Site-Specific Zn II Binding. *Eur. J. Inorg. Chem.* **2015**, *2015*, 3076−3086.

(73) Daumann, L. J.; Gahan, L. R.; Comba, P.; Schenk, G. Cadmium(II) Complexes: Mimics of Organophosphate Pesticide Degrading Enzymes and Metallo- β -Lactamases. *Inorg. Chem.* **2012**, *51*, 7669−7681.

(74) Daumann, L. J.; Comba, P.; Larrabee, J. A.; Schenk, G.; Stranger, R.; Cavigliasso, G.; Gahan, L. R. Synthesis, Magnetic Properties, and Phosphoesterase Activity of Dinuclear Cobalt(II) Complexes. *Inorg. Chem.* **2013**, *52*, 2029−2043.

(75) Seger, M. R.; Maciel, G. E. NMR Investigation of the Behavior of an Organothiophosphate Pesticide, Methyl Parathion, Sorbed on Clays. *Environ. Sci. Technol.* **2006**, *40*, 552−558.

(76) Silva, V. B.; Nascimento, L. L. Q.; Nunes, M. C.; Campos, R. B.; Oliveira, A. R. M.; Orth, E. S. Puzzling Reaction of Imidazole with Methyl Parathion: P=S versus P=O Mechanistic Shift Dilemma in Organophosphates. *Chem. - Eur. J.* **2019**, *25*, 817−822.

(77) Le Provost, R.; Wille, T.; Louise, L.; Masurier, N.; Muller, S.; Reiter, G.; Renard, P.-Y.; Lafont, O.; Worek, F.; Estour, F. Optimized Strategies to Synthesize B -Cyclodextrin-Oxime Conjugates as a New Generation of Organophosphate Scavengers. *Org. Biomol. Chem.* **2011**, *9*, 3026−3032.